THE ASTROPHYSICAL JOURNAL, 327:639–650, 1988 April 15

THE INTERNAL DYNAMICS OF THE PLANETARY NEBULAE IN THE LARGE MAGELLANIC CLOUD

MICHAEL A. DOPITA AND STEPHEN J. MEATHERINGHAM
Mount Stromlo and Siding Spring Observatories, Australian National University

B. LOUISE WEBSTER
School of Physics, University of New South Wales

AND

HOLLAND C. FORD
Space Telescope Science Institute
Received 1987 January 28; accepted 1987 October 13

ABSTRACT

The radial velocity and expansion velocity in the [O III] $\lambda5007$ line have been determined for a sample of 94 planetary nebulae (PN) in the Large Magellanic Cloud. In addition, densities and expansion velocities have been determined for a subset of 44 objects in both the Large and Small Magellanic Clouds using the [O II] $\lambda\lambda3727, 3729$ doublet. With a few notable exceptions, the [O II] expansion velocities are well correlated with, but are systematically higher than, the [O III] expansion velocities. For a given excitation class, there appears to be an upper limit to the density, in the sense that very high density objects are always of low excitation, but low-density objects can occur at any excitation. The population of PN in the Magellanic Clouds appears to form a sheet in dynamical age/excitation class/nebular density space, and therefore represents a two-parameter family. The implication of this is that the nebular parameters are entirely determined by the properties of the central star. This fact could represent the basis of a solution to the distance scale problem for Galactic PN.

Subject headings: galaxies: Magellanic Clouds — nebulae: planetary — stars: evolution

I. INTRODUCTION

There exists a substantial body of literature on the planetary nebula stage of stellar evolution. However, from an observational viewpoint much remains to be learned about the relationship between the expanding nebular shell and the planetary nebula nuclear star (PNn) during the evolution from an asymptotic giant branch (AGB) star to a hot, dense white dwarf. The major reason for this is that dynamical studies have, in the past, been exclusively concerned with the study of the Galactic PN, with all of the concomitant problems of uncertain distance scale, population type, and reddening. For example, no clear consensus has emerged on what is the evolutionary trend of expansion velocity. Robinson, Reay, and Atherton (1982) have suggested that the high- and low-mass PN have different expansion velocity/radius relationships. Phillips (1984) finds a monotonic relationship, with a small subset of large-diameter, slowly expanding nebulae. Some authors have suggested that a maximum in expansion velocity is reached at a radius of about 0.2 pc, with a slow decline to larger sizes (Smith 1969; Bohuski and Smith 1974; Sabbadin and Hamzaoglu 1982). The recent series of papers by Sabbadin and his collaborators has provided a great detail of knowledge on the evolution of the nebular properties of galactic PN with age (Sabbadin, Bianchini, and Hamzaoglu 1984; Sabbadin *et al.* 1984; Sabbadin 1986*a*, *b*).

The sample of planetary nebulae in the Magellanic Clouds offers notable advantages in evolutionary studies by furnishing us with a luminosity-limited sample at a known distance and with low line-of-sight reddening. This paper extends the results of our (almost) complete survey of the kinematics and internal dynamics of the PN in the Small Magellanic Cloud (Dopita *et al.* 1985), hereafter DFLW, to the population of Large Magellanic Cloud (LMC) planetary nebulae. The radial velocities are given in this paper, but the kinematical results are of sufficient interest in their own right to be the subject of a separate paper (Meatheringham *et al.* 1988*a*).

The results of this paper add to the homogeneous data set that is being accumulated on the Magellanic Cloud PN in order to provide an understanding of the post–asymptotic giant branch evolution. This data set includes Hβ photometry (Meatheringham, Dopita, and Morgan 1988), sizes from speckle interferometry and direct imaging (Wood, Bessell, and Dopita 1985; Wood, Dopita, and Bessell 1986; Wood *et al.* 1987), and spectrophotometric studies (Dopita *et al.* 1987*b*).

II. OBSERVATIONS AND DATA REDUCTION

a) Selection of Objects

The majority of the objects we have observed come from the list of Sanduleak, McConnell, and Philip (SMP) (1978), which includes many objects previously known as planetary nebulae (Henize and Westerlund 1963). This list was supplemented by a few objects from the Jacoby (J) (1980) list, many of which are exceedingly faint and difficult to observe. Some of these objects appear to show no trace of [O III] emission, but rather a faint structured continuum. Since these objects were selected on the basis of their apparent [O III] emission in narrow-band images, they are unlikely to be low-excitation PN. Indeed, they may not be PN at all, but this conclusion needs to be confirmed with low-dispersion spectroscopy. Recently, Morgan and Good (MG) have undertaken a deep search of high-dispersion UK Schmidt telescope objective prism material with the aim of extending the sample of objects to a wider search region and to lower luminosities. A few of the brightest of these have also been observed. All appear to be bona fide PN, frequently in an advanced evolutionary state. The excitation classifications were made by Morgan (1984) on the basis of UK Schmidt objective prism material. Morgan adapted the classification scheme of Feast (1968) which was in turn based on the classification originally proposed by Aller (1956). On average the excitation classification should be good to about one class, although errors may be larger than this in the case of faint objects.

b) The Observations

We have used three telescopes, two spectrographs, and two photon-counting systems in this study. Observations in the [O III] $\lambda 5007$ line were made in 1983 October and November and 1984 October on the 1.0 m telescope at Siding Spring Observatory, and observations in 1985 January used the 2.3 m advanced technology telescope also at Siding Spring. Both these telescopes are operated by the Australian National University, and the Perkin-Elmer échelle spectrograph was used on both telescopes as the dispersing element, with the photon counting array as detector. Supplementary [O III] observations of the fainter objects were made in 1983 December on the 3.9 m Anglo-Australian Telescope using its RGO spectrograph and the image photon counting system as the detector.

The instrumental parameters and the reduction procedures for the [O III] data are identical to those described in DFLW and will not be described again here. The resolution of both systems are very similar, 11.5 km s^{-1} FWHM for the échelle spectrograph, and 11.75 km s^{-1} for the RGO spectrograph. The estimated errors in determination of the radial velocity are ± 1.5 km s^{-1} for the 1.0 m observations, ± 0.6 km s^{-1} for the 2.3 m data, and ± 0.3 km s^{-1} in the case of the AAT data.

The observations in the [O II] $\lambda\lambda 3727$, 3729 doublet were made on the 3.9 m Anglo-Australian Telescope in 1985 January. The RGO spectrograph was used with its 82 cm camera with a grating of 1200 lines mm^{-1} blazed at J and operating in second order. The slit width of 80 μm gave a system resolution (FWHM) of 11.4 km s^{-1}. As for the [O III] data the spectral line profiles were fitted using the multiple Gaussian fitting routines of the SPECTRE code (Pelat, Alloin, and Fosbury 1981). Up to four Gaussian components were used for each line, but the widths and spacings of the two doublet components were kept fixed, relative to each other. Figure 1 shows the result of this fitting process on a representative PN, both for the [O III] line and the [O II] doublet.

III. RESULTS

a) The [O III] $\lambda 5007$ *Data*

In Tables 1 and 2 we present the excitation class and Hβ flux (where known) for the LMC PN that we observed. Also given are the measured [O III] $\lambda 5007$ radial velocities with respect to the local standard of rest and the measured expansion velocities in this spectral line. Here we follow the definitions given in DLFW, and we refer the reader to that paper for a full discussion. Briefly, the expansion velocity is defined to be half the full width at 10% maximum. This figure was found from models to give an answer which is largely independent of brightness distribution within the nebula. If the more usual FWHM definition had been used, then, for example, nebulae with two bright ansae would have apparently different expansion velocities depending on whether these ansae lie in the plane of the sky or along the line of sight. The 10% figure adopted ensures that the expansion velocity of these unresolved objects is determined by the fastest gas in the outer ionized shell. This figure should be rather closely related to the maximum line splitting observed in resolved objects. For those objects fitted by a single Gaussian (in Table 1), the relationship between the expansion velocity, $V_{\rm exp}$, and full width at half-maximum (FWHM), ΔV, is given by $V_{\rm exp} = 0.911\,\Delta V$. In the case of those objects showing two components, which are most likely to show a bipolar structure when resolved, our definition of expansion velocity measures half the velocity difference between the (low-velocity) 10% maximum point on the low-velocity component with radial velocity $V_{\rm LSR}(1)$ and FWHM

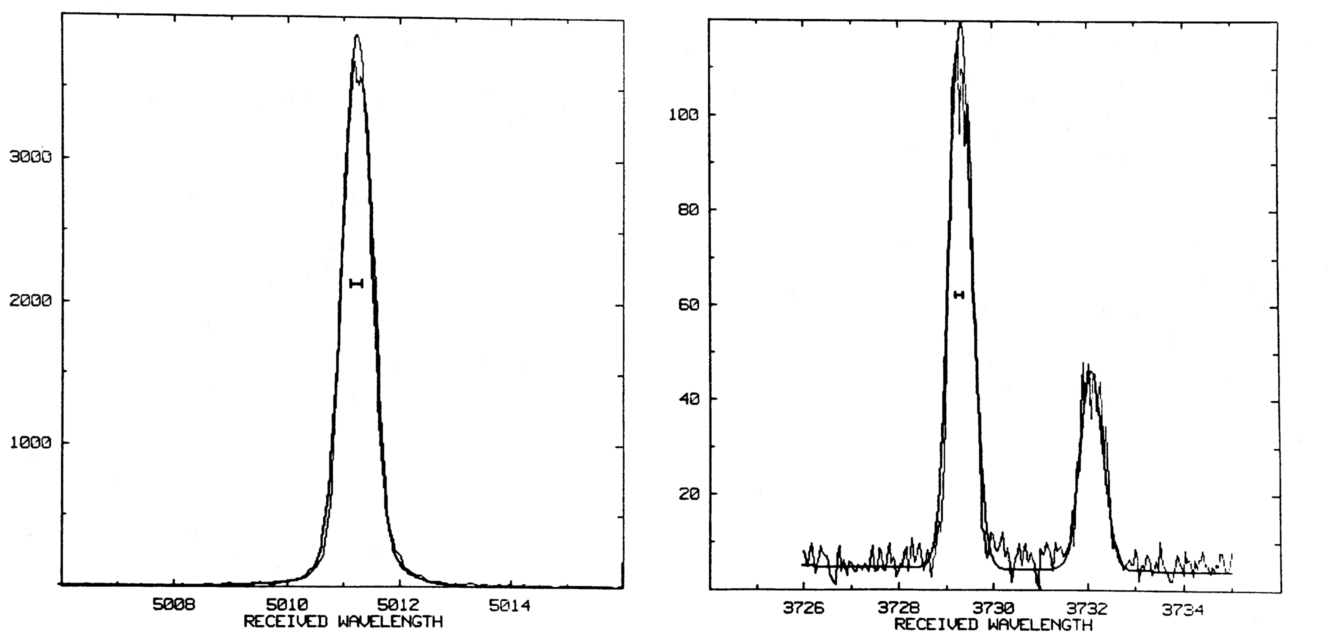

FIG. 1.—Observed line profiles in [O III] $\lambda 5007$ (*left*) and the [O II] $\lambda\lambda 3727$, 3729 doublet (*right*) for a representative LMC planetary nebula, SMP 6. Also shown is the multiple Gaussian line fits to these profiles. The bars represent the instrumental full width at half-maximum.

TABLE 1

VELOCITY AND FLUX DATA FOR LMC PLANETARY NEBULAE FITTED BY A SINGLE GAUSSIAN COMPONENT

Object Name[a]	Excitation Class[b]	$\log (F_{H\beta})^c$ (ergs, cm^{-2} s^{-1})	V_{LSR} (km s^{-1})	V_{exp} (km s^{-1})	Object Name[a]	Excitation Class[b]	$\log (F_{H\beta})^c$ (ergs, cm^{-2} s^{-1})	V_{LSR} (km s^{-1})	V_{exp} (km s^{-1})
SMP 1	4	−12.46	209.1	17.2	SMP 57	3–6	−13.41	297.6	32.5
SMP 2	...	−13.18	248.2	9.9	SMP 58	4	−12.48	264.2	18.8
SMP 3	...	−12.48	172.0	20.0	SMP 60	9.5	−13.50	207.0	58.3
SMP 4	...	−13.52	282.9	37.9	SMP 61	4	−12.48	178.4	29.3
SMP 6	7	−12.67	249.0	28.6	SMP 62	6	−12.31	223.6	34.6
SMP 7	6	−13.12	204.8	44.7	SMP 63	4–5	−12.48	248.8	16.7
SMP 8	2	−12.74	277.1	25.2	SMP 65	2–5	−13.31	195.7	17.8
SMP 9	6–7	−13.38	270.7	22.9	SMP 66	5–6	−12.95	289.2	23.1
SMP 13	6	−12.82	212.3	46.1	SMP 67	1	−12.81	274.1	27.9
SMP 14	3–7	−13.69	236.9	51.5	SMP 69	8–9	−13.17	289.9	44.3
SMP 15	5–6	−12.66	188.0	41.2	SMP 71	6–7	−12.86	201.2	28.0
SMP 16	8	−13.30	237.5	33.0	SMP 73	6	−12.54	225.6	25.9
SMP 18	2–6	−13.36	228.7	27.4	SMP 74	5	−12.66	253.6	35.1
SMP 19	7	−12.73	220.2	28.6	SMP 77	1	−12.78	328.2	12.9
SMP 20	2	−13.37	273.1	25.8	SMP 78	6	−12.58	240.7	33.4
SMP 23	4	−12.68	267.1	21.6	SMP 79	5	−12.63	215.1	37.2
SMP 24	...	−13.77	254.7	56.4	SMP 81	5	−12.61	242.2	32.6
SMP 27	3–6	−13.40	258.2	33.3	SMP 84	4	−12.63	235.0	46.2
SMP 28	6–7	−13.35	233.7	55.0	SMP 85	1	−12.42	217.0	11.3
SMP 29	7	−12.71	228.2	35.9	SMP 87	8–9	−12.91	264.6	37.4
SMP 31	0	−12.91	248.1	5.1	SMP 88	9	−13.26	211.0	24.7
SMP 32	8–9	−12.80	240.2	42.3	SMP 89	5	−12.61	261.2	25.2
SMP 33	6–7	−12.81	253.9	30.8	SMP 91	7	−13.55	295.3	45.3
SMP 36	5–6	−12.72	247.6	34.6	SMP 92	6	−12.54	256.4	29.3
SMP 37	7	−12.85	255.2	39.2	SMP 95	5–7	−13.47	290.9	31.2
SMP 38	5	−12.62	225.4	34.5	SMP 96	9	−13.34	239.4	60.9
SMP 42	5–6	−13.11	273.4	37.9	SMP 99	5	−12.54	248.8	25.3
SMP 45	6	−13.17	275.0	36.8	SMP 100	6	−12.86	270.1	46.4
SMP 46	6	−13.60	258.0	26.1	SMP 102	7	−13.22	286.5	41.2
SMP 48	3–4	−12.43	240.8	15.8	J5	1	−13.25	262.9	25.4
SMP 50	5	−12.71	284.1	35.0	J33	...	...	231.2	43.2
SMP 51	3–9	...	256.4	23.3	A0	...	...	288.5	34.3
SMP 52	5	−12.52	256.9	36.3	A3	...	...	272.9	20.3
SMP 53	5	−12.62	261.8	25.0	A22	...	...	236.6	22.1
SMP 55	0.5	−12.66	194.7	6.0	A24	...	...	267.2	34.6
SMP 56	1	−13.13	276.1	10.3	A54	...	...	282.8	33.3

[a] For nomenclature, see § II*a*.

[b] Excitation class from Morgan 1984.

[c] Flux from Meatheringham *et al.* 1988*b*.

width $\Delta V(1)$, and the corresponding high-velocity point on the high-velocity component with radial velocity $V_{LSR}(2)$ and width $\Delta V(2)$:

$$V_{exp} = 0.455[\Delta V(1) + \Delta V(2)] + 0.5\,|\,V_{LSR}(1) - V_{LSR}(2)\,|$$

In Table 2 we give the mean radial velocity and the expansion velocity for the objects observed. Two or more radial velocities are given for those objects which required more than one Gaussian component for a fit. Two expansion velocities are given for those objects fitted by three or four components (double shell objects), but in the analysis below, the expansion velocity used is that measured by the principal components of the fit. Also given in Table 2 are the parameters which characterize the individual Gaussians of the fit: radial velocity, width, and integrated intensity with respect to the principal component.

The existence of PN in the LMC which show extremely high velocity motions has already been reported (Dopita, Ford, and Webster 1985). However, Table 2 suggests that the existence of a high-velocity outer shell or bipolar flow is not very unusual among the fainter (optically thin?) PN. Several examples are shown in Figure 2, which serves to emphasize how the faint tails of the profiles are difficult to observe, even though they may contribute a substantial fraction of the total flux.

The agreement between the radial velocities given here and those found in earlier studies is very good. For a discussion, see Meatheringham *et al.* 1988.

b) The [O II] λ3727, 29 *Data*

The [O II] data were collected on a subsample of objects in both the Large and Small Magellanic Clouds, chosen to cover as wide a range of excitation class and flux as possible. Size estimates based on preliminary density and flux estimates were used to select objects for subsequent speckle interferometry observations (Wood, Bessell, and Dopita 1985; Wood, Dopita, and Bessell 1986).

The electron densities determined from the observed λ3727/λ3729 line ratio with the aid of five-level model atom calculations using collisions strengths of Pradhan (1976) and the transition probabilities of Zeippen (1982). The densities given are for an assumed electron temperature of 10,000 K. The derived expansion velocities and densities are summarized in Tables 3 and 4. Most of the line profiles obtained were adequately fitted by a single Gaussian component, but for the rest, two components were required. For these cases, expansion

TABLE 2

Velocity and Flux Data for LMC Planetary Nebulae Fitted by Multiple Gaussian Components

Object Name[a]	Excitation Class[b]	$\log (F_{H\beta})$[c] ($\mathrm{ergs\ cm^{-2}\ s^{-1}}$)	$\langle V_{LSR} \rangle$ ($\mathrm{km\ s^{-1}}$)	V_{exp} ($\mathrm{km\ s^{-1}}$)	V_{LSR} ($\mathrm{km\ s^{-1}}$)	ΔV ($\mathrm{km\ s^{-1}}$)	A_{rel}[d]
SMP 5	1	−12.85	271.0	20.8	270.7	7.5	1.000
					271.7	35.6	0.545
				(76.6)	271.2	83.2	0.190
SMP 10	6–7	−13.15	207.0	47.0	189.7	33.1	1.000
					224.5	31.8	0.901
SMP 11	7[e]	−13.15	249.4	122	237.0	54.5	1.000
					204.5	96.7	0.694
					296.6	56.3	0.583
					354.7	84.5	0.153
SMP 21	7	−12.76	244.8	49.1	249.8	37.4	1.000
					209.4	25.8	0.272
				(128)	237.9	141	0.476
SMP 30	8	−13.45	264.9	40.9	270.1	58.2	1.000
					258.5	18.9	0.831
SMP 35	5	−12.81	295.0	41.3	281.6	31.5	1.000
					314.0	23.6	0.673
SMP 40	7	−13.25	238.9	54.5	238.7	29.9	1.000
					261.8	64.3	0.623
					210.4	118	0.491
SMP 41	6	−13.33	244.2	51.7	240.3	48.0	1.000
					278.7	23.4	0.207
				(155)	205.9	136	0.133
					335.4	61.6	0.058
SMP 47	6–7	−12.52	258.3	50.1	254.9	55.0	1.000
				(148)	195.7	115	0.089
					297.8	99.3	0.361
SMP 49	6	−13.35	232.2	38.1	222.8	33.3	1.000
					248.6	22.0	0.116
SMP 54	8	−13.51	264.3	42.3	250.4	31.1	1.000
					279.8	29.7	0.837
				(96.2)	214.4	56.3	0.123
					299.3	61.7	0.198
SMP 76	3	−12.54	262.8	29.0	264.0	22.8	1.000
					273.7	30.2	0.554
SMP 82	3–4	...	239.6	38.4	238.9	66.4	1.000
					240.9	15.9	0.513
SMP 83	8–9[e]	−12.65	274.5	82.9	232.5	57.7	1.000
					323.9	41.8	0.839
				(142)	212.3	104	0.118
					348.9	57.6	0.193
SMP 94	7[e]	−12.99	259.4	40.7	(Symbiotic star)		
SMP 97	8–9	−12.85	271.8	46.1	287.8	31.5	1.000
					255.3	32.9	0.976
SMP 101	7–8	−12.81	266.0	47.3	250.2	40.0	1.000
					284.5	26.3	0.699
J26	...	...	230.3	61.7	243.9	60.2	1.000
					228.1	58.0	0.970
J38	...	...	265.6	36.9	265.1	40.5	1.000
				(74.1)	245.1	52.0	0.208
					306.6	43.3	0.111
J41	...	...	240.0	29.3	232.1	29.7	1.000
					247.7	61.5	0.833
A4	...	...	254.2	68.8	268.2	54.0	1.000
					218.5	42.7	0.393
A46	...	...	243.4	52.5	232.3	39.0	1.000
					285.8	37.7	0.464

[a] For nomenclature, see § II*a*.

[b] Extinction class from Morgan 1984.

[c] Flux from Meatheringham, Dopita, and Morgan 1988.

[d] Area under Gaussian, relative to main component.

[e] See discussion in Dopita, Ford, and Webster 1985.

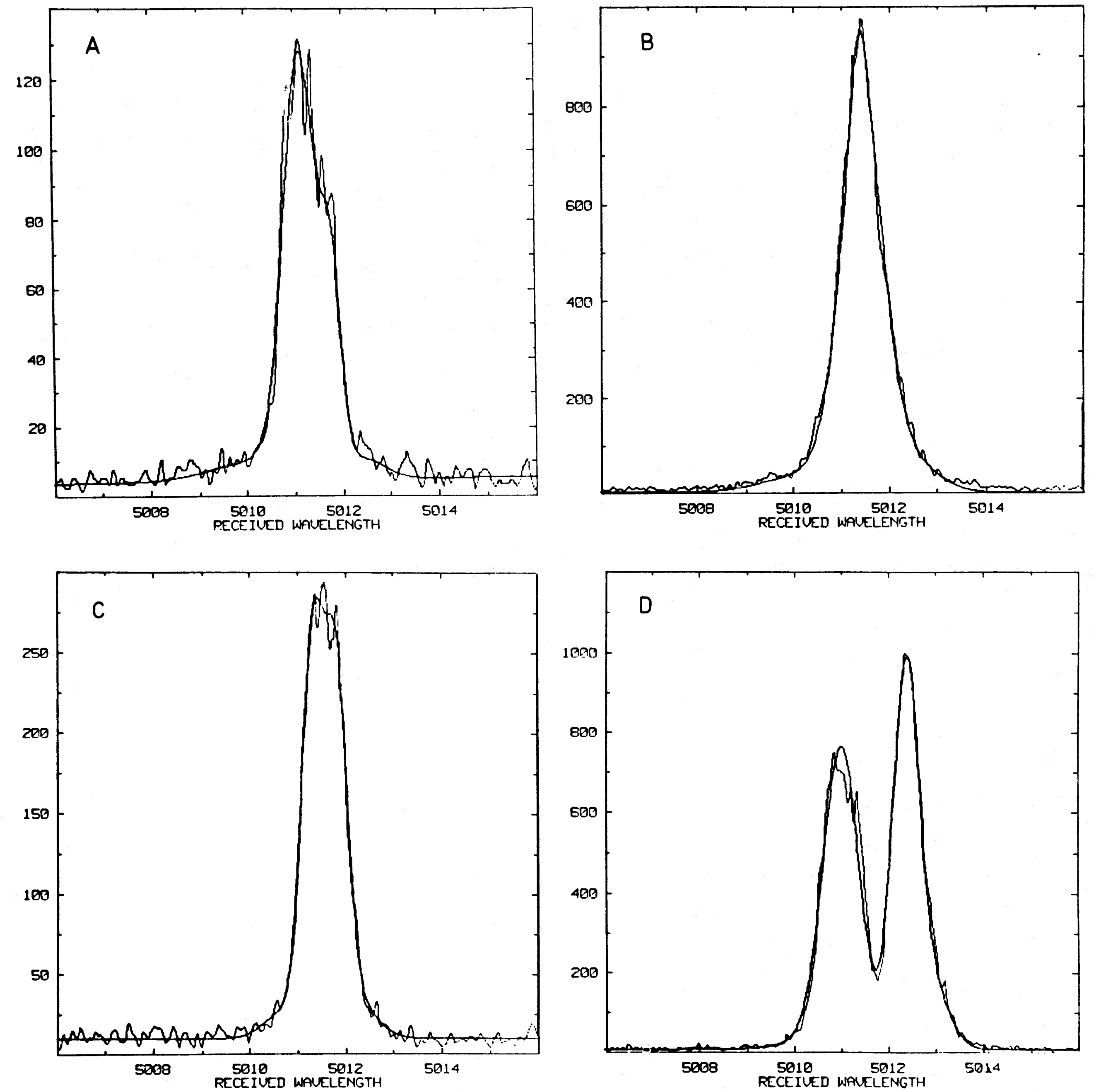

FIG. 2.—Observed [O III] line profiles for those objects showing evidence for a high-velocity outer shell of matter. These are: A, SMP 41; B, SMP 47, C; SMP 54, D; SMP 83. Although the faint wings of the profile contain an appreciable fraction of the total flux, they are nevertheless difficult to observe.

velocities were determined in the same manner as for the [O III] data. It is also possible to determine the electron densities for each of the components of the fit, and these are given separately in Tables 3 and 4. Such cases probably correspond physically to a bipolar morphology, since integration over a spherical expanding shell can, at best, produce only a marginal resolution into two components.

The [O II] doublet ratios and densities of 32 Magellanic Cloud PN have recently been measured by Barlow (1987), but at a resolution which did not permit a measurement of internal motions. These are also given in the tables. In general, the agreement is good, but there are one or two discrepant results. For those objects observed in common, we believe that our results, with higher resolution, exposure time and total counts, should be more reliable. Exceptions to this are SMC SMP 13, 14, and 27 and LMC SMP 47 and 50 where the signal is low in our observations.

c) *A Comparison of the* [O III] *and* [O II] *Expansion Velocities*

The [O II] and [O III] expansion velocities are, in general, well correlated (see Fig. 3). However, notable exceptions to the correlation are SMP 26 in the SMC, and SMP 40, 83, and 96 in the LMC. These are all low-density nebulae of high excitation and show anomalously high [O III] expansion velocities. These

TABLE 3

Expansion Velocities and Densities in the SMC Planetary Nebulae Derived from the [O ii] Doublet

Object Name[a]	Excitation Class[b]	V_{exp}[O iii] (km s^{-1})	V_{exp}[O ii] (km s^{-1})	$I(\lambda3729)/I(\lambda3726)$	n_e (cm^{-3})
SMP 1	0.5	15.4	16.1	0.42	10500
SMP 2	6	32.2	...	0.59[c]	2900
SMP 3	4	32.9	...	0.68[c]	1800
SMP 5	6–7	29.2	43.6	0.56	3500
				0.54[c]	3900
SMP 6	4	21.9	...	0.38[c]	26000
SMP 9	7–8	37.9	...	1.19[c]	270
SMP 13	4	28.1	29.8	0.69	1800
				0.45[c]	7200
SMP 14	6	48.9	62.7	0.54	3900
				0.58[d]	3000
				0.56[c]	3300
SMP 15	2–4	15.2	20.8	0.35	65000
				0.43[c]	8800
SMP 16	0	11.7	8.8	0.40	15500
SMP 17	3–5	24.2	31.5	0.50	5100
				0.50[c]	4600
SMP 18	0.5	12.7	19.2	0.46	7300
SMP 19	7	30.1	...	0.53[c]	3920
SMP 20	1–2	20.2	30.3	0.37	35000
				0.34	70000
SMP 21	3	35.2	...	0.35[c]	40000
SMP 22	8	50.9	51.2	0.56	3500
				0.48[d]	5100
				0.52[c]	4200
SMP 24	1–2	16.6	35.6	0.46	6800
				0.42[c]	9800
SMP 26	8	50.6	41.0	0.79	1300
SMP 27	3	31.3	36.3	0.49	5400
				0.46[c]	6400
SMP 28	8	54.4	...	0.70	1900

[a] For nomenclature, see § II*a*.
[b] Excitation class from Morgan 1984.
[c] From Barlow 1986.
[d] Where two values are given, the second refers to the higher velocity component.

are likely to be nebulae which are optically thin in some directions. In such nebulae the low-excitation lines would originate near ionization fronts close to a central reservoir of H i, whereas the [O iii] emission is found in strongly accelerated flows toward the outer optically thin portions of the nebula. The LMC nebula, SMP 63, is anomalous in the other sense but is not otherwise remarkable.

It might have been expected that these data would show evidence for ionization stratification effects, particularly for the low-excitation nebulae below class 3, where, according to photoionization models, the O^{2+} zone becomes confined to the inner region of the nebula. One would therefore expect the [O iii] expansion velocities to lie well below the [O ii] expansion velocities. In fact, no evidence of this effect is found. However, there is some evidence for a stratification effect at *all* excitation classes, because the [O ii] expansion is systematically higher than that found for the [O iii] line. The slope of the correlation in Figure 4 is 0.818 ± 0.035. Since the [O ii] emission always arises near the outer boundary of the ionized region, this indicates that the nebula reaches its maximum velocity of expansion in the outer regions. Since O^{2+} is usually the dominant ionization stage, the ratio of measured expansion velocities gives, in effect, an estimate for the thickness of the ionized shell, provided that there exists an outwardly increasing velocity gradient, $V_{exp} \propto R$, such as observed by Wilson (1950). Thus the fractional thickness of the ionized shell, $\Delta R/R_{neb}$, is of order 0.18. This should be compared with the mean value of about 0.15 found for Galactic PN (Daub 1982; Phillips 1984).

IV. OBSERVATIONAL CORRELATIONS

a) Correlations between Expansion Velocity, Excitation Class, and Flux

In DFLW it was shown that a good correlation exists between the expansion velocity and the excitation class for

TABLE 4

Expansion Velocities and Densities in the LMC Planetary Nebulae Derived from the [O ii] Doublet

Object Name[a]	Excitation Class[b]	V_{exp}[O iii] (km s^{-1})	V_{exp}[O ii] (km s^{-1})	$I(\lambda3729)/I(\lambda3726)$	n_e (cm^{-3})
SMP 1	4	17.2	23.1	0.55	3600
SMP 5	1	20.8	20.9	0.67	2000
SMP 6	7	28.6	39.3	0.40	14000
				0.54[c]	3850
SMP 8	2	25.2	27.1	0.48	6300
SMP 15	5–6	41.2	51.0	0.49	5400
SMP 20	2	25.8	36.3	0.78	1300
SMP 21	7	49.1	55.4	0.45	7800
				0.62[c]	2400
SMP 23	4	21.6	38.5	0.48	5900
SMP 29	7	35.9	49.3	0.50	4900
				0.44	8200
SMP 31	0	5.1	14.4	0.44	8800
SMP 37	7	39.2	...	0.45[c]	7300
SMP 38	5	34.5	...	0.35[c]	13000
SMP 32	8–9	42.3	51.4	0.60	2800
SMP 40	6	51.7	39.1	0.81	1200
SMP 44		...	57.4	0.78	1300
				0.81[d]	1100
SMP 45	6	36.8	47.2	0.76	1400
				0.76[d]	1400
SMP 46	6	26.1	42.6	0.54	4000
SMP 47		50.1	58.4	0.50	5100
				0.62[c]	2500
SMP 50	5	35.0	55.7	0.50	5000
SMP 52	5	36.3	42.8	0.59	2900
SMP 55	0.5	6.0	18.2	0.37	40000
SMP 58	4	18.8	...	0.35	66000
SMP 61	4	29.3	33.3	0.36	40000
				0.37[c]	30000
SMP 62	6	34.6	47.5	0.48	6200
				0.49[c]	4800
SMP 63	4–5	16.7	48.1	0.43	9800
				0.44[c]	7700
SMP 67	1	27.9	42.7	0.55	3700
SMP 76	3	29.0	32.9	0.40	14500
SMP 77	1	12.0	17.4	0.56	3500
SMP 78	6	33.4	36.7	0.52	4300
				0.51[c]	4500
SMP 83	8–9	82.9	80.9	0.64	2300
				0.84[d]	1100
				0.59[c]	2600
SMP 85	1	11.3	11.2	0.34	High
SMP 87	8–9	37.4	39.8	0.70	1800
SMP 89	5	25.2	36.8	0.50	4900
				0.53[c]	3900
SMP 92	6	29.3	37.4	0.43	10000
SMP 96	9	60.9	37.0	0.61	2700
J5	1	25.4	25.6	0.84	1100

[a] For nomenclature, see § II*a*.
[b] Excitation class from Morgan 1984.
[c] From Barlow 1986.
[d] Where two values are given, the second refers to the higher velocity component.

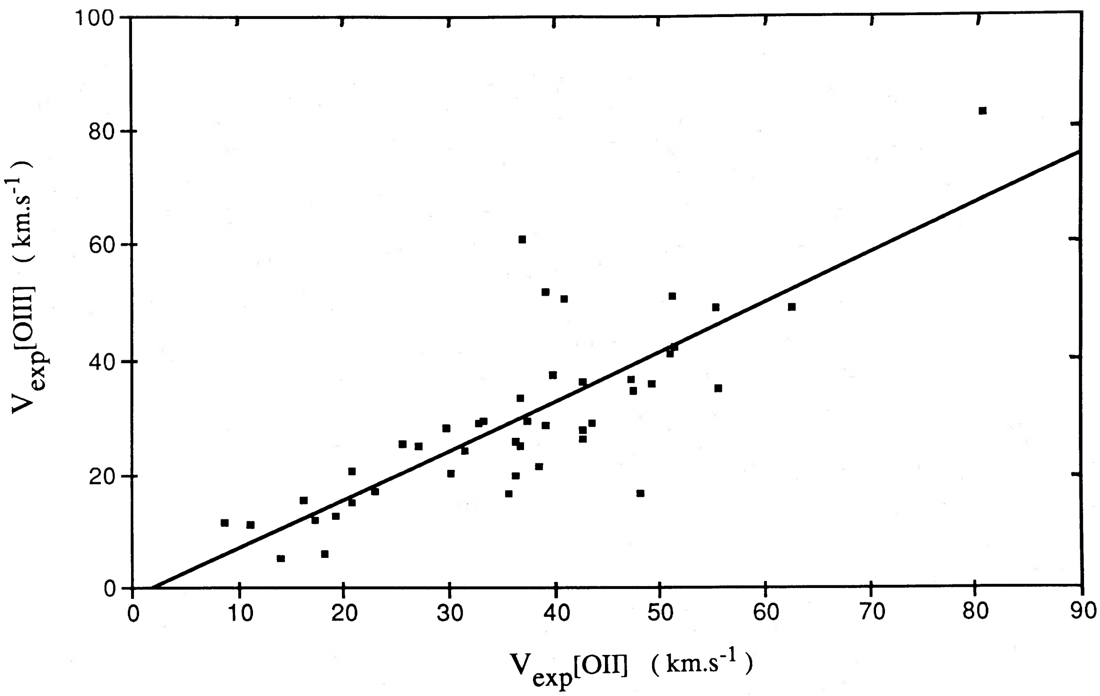

FIG. 3.—The correlation between the measured [O II] and [O III] expansion velocities for PN in both the LMC and SMC. The [O II] expansion velocity is well correlated with, but systematically larger than, the [O III] expansion velocity.

SMC planetary nebulae. Such a correlation also applies to the LMC population (see Fig. 4). However, it is apparent from the Hβ flux determinations (Meatheringham, Dopita, and Morgan 1988) that some correlation also exists between this quantity and the expansion velocity. Although this is best for the SMC planetaries (Dopita *et al.* 1987*a*), it is still apparent in the LMC population where the correlation coefficient is 0.34. The best-fit correlation between the expansion velocity, $V_{\rm exp}$, and a combination of both of the excitation class and Hβ flux of the form

$$V_{\rm exp} = a + bE + c \log (F_{{\rm H}\beta}) , \tag{1}$$

where E refers to the excitation class and a, b, and c are constants, has the parameters $a = -58$, $b = 3.53$, and $c = -5.56$. With these values an RMS velocity difference of 8.3 km s^{-1} between the observed and the fitted expansion velocities is found (see Fig. 5).

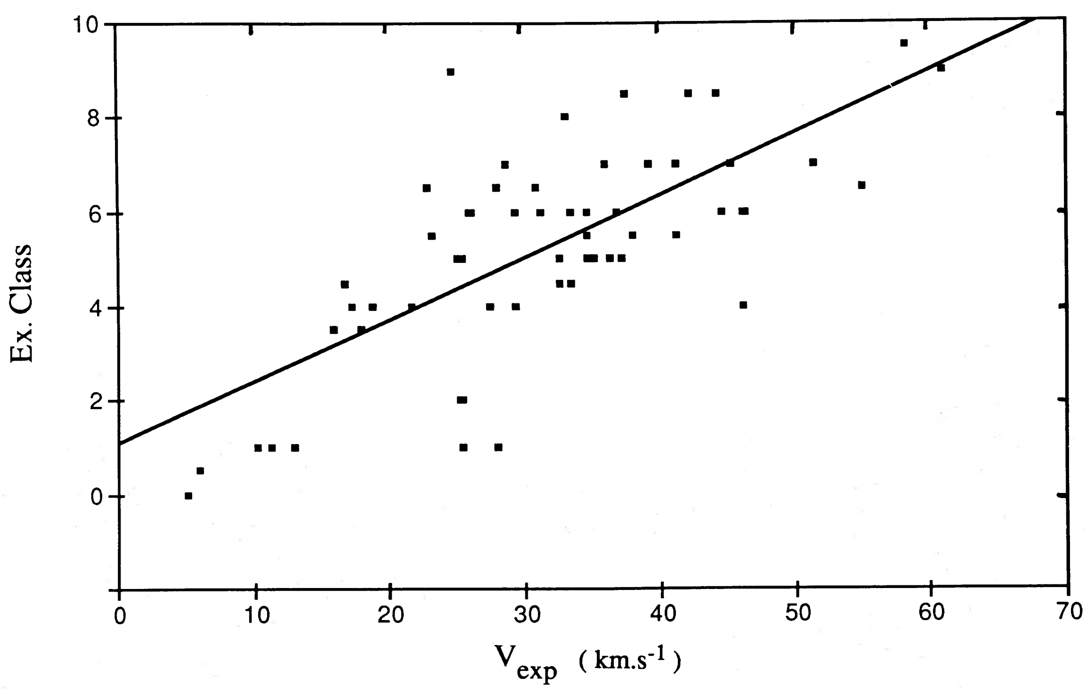

FIG. 4.—The correlation between excitation class and [O III] expansion velocity for those LMC planetaries fitted by a single Gaussian component

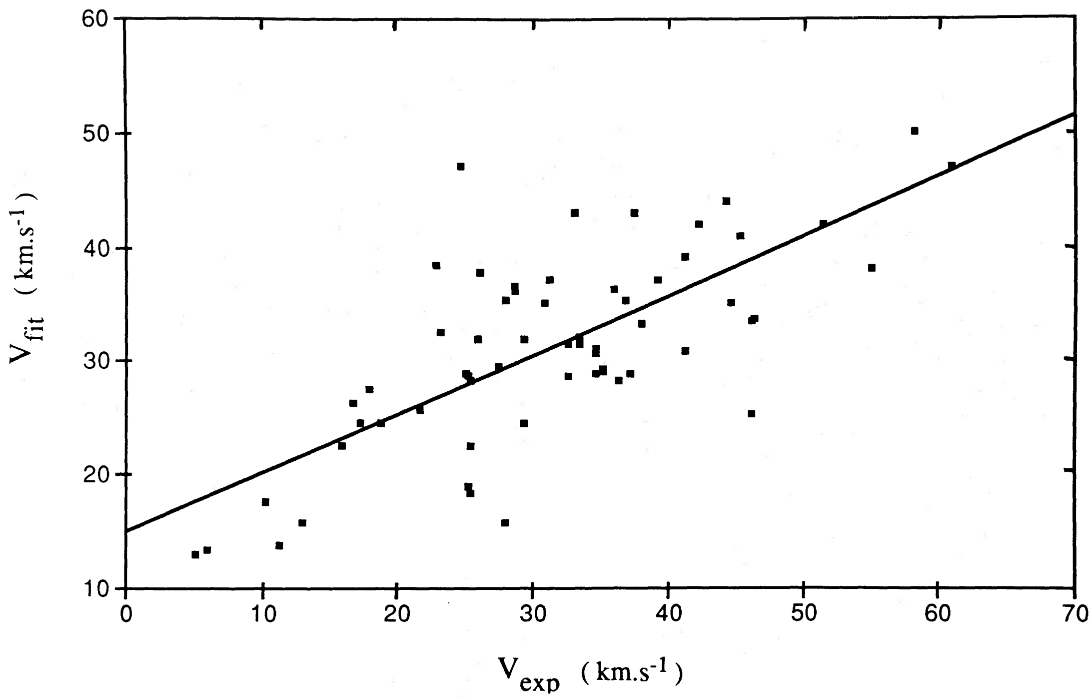

FIG. 5.—The expansion velocity given by eq. (1) compared with the observed [O III] expansion velocity. The fit is much less good than for the SMC planetaries, indicating that the latter group of objects may be drawn from a more homogeneous population.

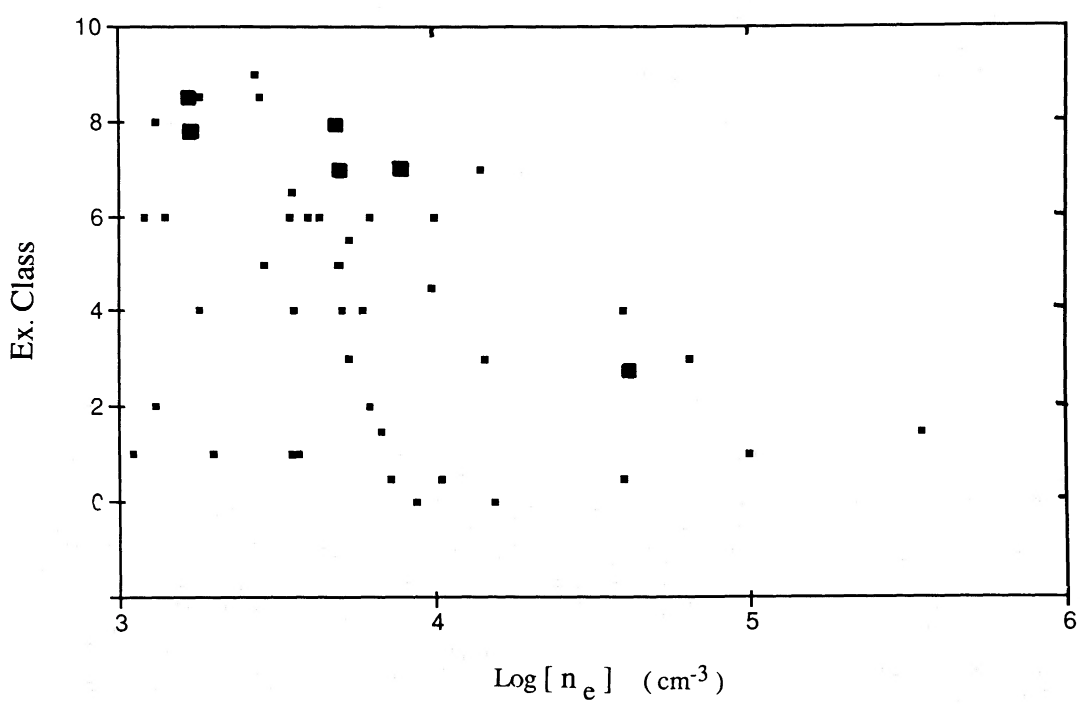

FIG. 6.—The excitation class/electron density plane for LMC and SMC planetaries. Planetaries known to be of type I are marked with larger symbols. Note the forbidden region at high density and excitation. It is argued in § V that, at a given mass of the PNn, the evolutionary track proceeds from lower right to upper left in a direction somewhat parallel to the upper envelope of observed points in this diagram.

b) The Density/Excitation Correlation

Excitation class and density are not well correlated in the sample of nebulae of Tables 3 and 4 (see Fig. 6). However, there is a clear upper limit to the permissable density at a given excitation class. No high-density, high-excitation nebulae are observed. Excitation class depends to some extent on the ionization parameter, but it is, of course, more affected by the stellar effective temperature. The absence of high-density, high-excitation objects appears therefore to point to a real lack of high-temperature PNn in compact nebulae.

c) The Mass/Density Correlation

In the limit of low reddening, the observed flux, $F(\mathrm{H}\beta)$, and the mean electron density, n_e, can be used to derive the ionized mass of the PN from the formula

$$M_{\mathrm{neb}} = 4\pi D^2 F(\mathrm{H}\beta)(1 + 4y)m_{\mathrm{H}}/\alpha_{\mathrm{eff}}\, h\nu n_e\ , \quad (2)$$

where D is the distance, $y = N(\mathrm{He})/N(\mathrm{H})$, and α_{eff} is the effective recombination coefficient of hydrogen for the emission of Hβ photons of energy $h\nu$. However, the mean electron density is not directly determined, only its emission weighted mean from the [O II] forbidden line ratio. These are related through $n_e(\mathrm{forbid}) = n_e \epsilon^{1/2}$, where ϵ is the volume filling factor of matter. For Galactic PN, the filling factor appears to depend very little, if at all, on density, and lies between $0.3 < \epsilon < 1.0$. Indeed the best correlation between densities derived from flux measurements and those derived from the [O II] forbidden line is found for $\epsilon = 1.0$ (Seaton 1966; Pottasch 1980). In what follows we derive the mass on the assumption of $\epsilon = 1.0$, recognizing that this could cause the masses to be systematically overestimated. On the other hand, our Hβ fluxes are uncorrected for reddening, and this will tend to lead to an underestimate in the mass.

Substituting numerical values in equation (2) yields

$$\log (M_{\mathrm{neb}}) = 15.5 + \log F(\mathrm{H}\beta) - \log n_e\ . \quad (3)$$

We have used the figures given in Tables 3 and 4 to derive the nebular mass directly from this equation.

The correlation between the density and the ionized mass so derived is shown on Figure 7. The linear regression relation is

$$\log (M_{\mathrm{neb}}) = 1.36 \pm 0.30 - 0.626 \pm 0.079 \log n_e \quad (4)$$

and the correlation coefficient is 0.774. The discrepant point in the lower left is LMC; SMP 50.

d) Dynamical Age/Momentum Correlation

This relationship, and its physical basis, have been discussed elsewhere (Dopita *et al.* 1987*a*), and this discussion will not be further developed here. In that paper, on the basis of sizes derived from speckle interferometry (Wood, Bessell, and Dopita 1985) and on high-speed direct imaging (Wood *et al.* 1987), it was found that the Magellanic Cloud PN conform to a relationship of the form

$$\tau_{\mathrm{dyn}} = 890(M_{\mathrm{neb}}\, V_{\mathrm{exp}})^{0.6}\ \mathrm{yr} \quad (5)$$

where M_{neb} is the mass in solar units and V_{exp} is the [O III] expansion velocity in km s^{-1}. The dynamical age has been directly established for very few of the objects in Tables 3 and 4. However, the age is such a vital parameter in understanding the evolution, that here we adopt equation (5) as being established and use the derived mass and observed expansion velocity to determine the dynamical age.

e) The Age/Density/Excitatio. lane

The dynamic age as derived above is strongly correlated with either the excitation class, E, (correlation coefficient 0.575)

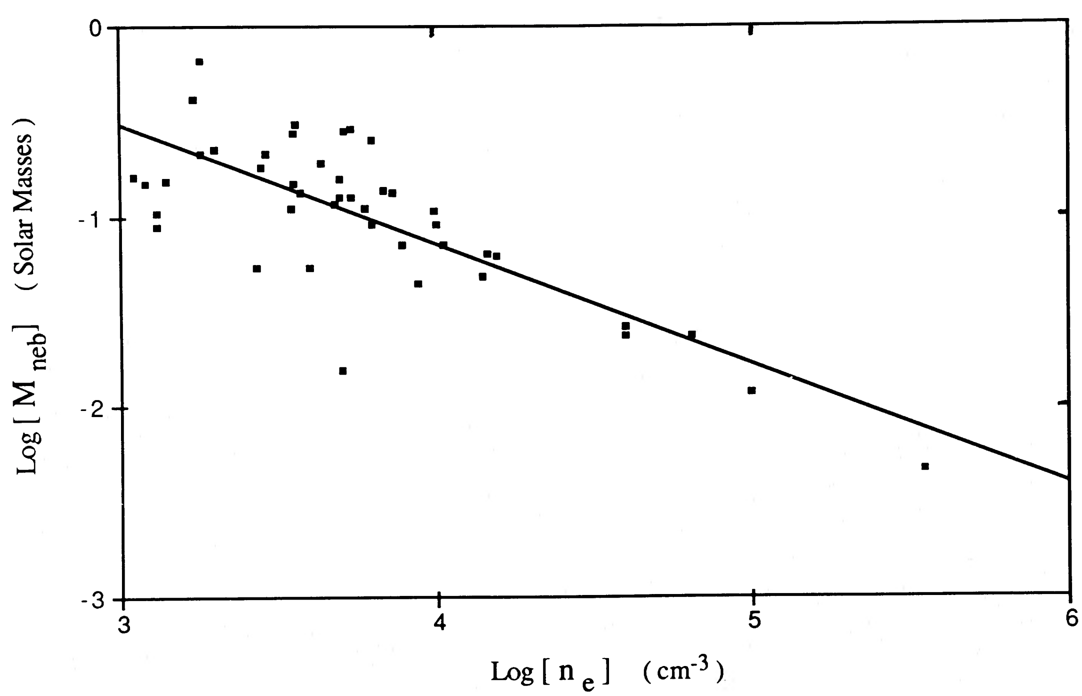

FIG. 7.—The correlation between ionized mass and density for LMC and SMC planetaries

or with the logarithm of the electron density (correlation coefficient -0.811). We were therefore encouraged to find whether the PN are, in fact, a two-parameter family in these variables. In fact, this turns out to be the case. Figure 8 shows that the observed points fall in a plane in the dynamical age/density/excitation class space defined by

$$\log(\tau_{\rm dyn}) = 4.70 \pm 0.23 + 0.0375 \pm 0.0106E - 0.441 \pm 0.05 \log n_e \, . \quad (6)$$

The fit between the dynamic age computed using equation (6) and the observed value is shown in Figure 9.

V. DISCUSSION

The observed correlations discovered in this paper, in Dopita *et al.* (1987*a*) and in Wood *et al.* (1987) put very powerful restraints on the possible models of the evolution of planetary nebulae and their central stars. Although fairly good correlations have been found connecting individual nebular quantities such as nebular mass and radius or density, or between excitation class and velocity of expansion, when the all-important variable of nebular age is considered two nebular parameters are required to give a good correlation. In the two particular cases we have discussed here, the topology of the observed surface appears to be a flat sheet. These are dynamical age versus mass and velocity of expansion and dynamical age versus density and excitation class. However, dynamical age versus excitation class and Hβ flux also produces a sheet-like correlation, albeit distorted.

What is the physical meaning of such dual correlations? Firstly, the Hβ flux should correlate well with the luminosity of the PNn, at least for the optically thick nebulae. Second, the definition of the excitation class as adopted by Morgan (1984) ensures that this is closely related to the Zanstra temperature of the PNn, provided that the ionization parameter of the nebula is high enough. Nebulae in which the fading of the central star is sufficient to allow the excitation to drop will have been strongly discriminated against in our effectively flux-limited sample. The mass, radius, and density of the ionized region are closely correlated and are clearly related in some way with age. The position of a PN on such dual correlations should therefore depend principally on the properties of the PNn.

The low-excitation/high-density PN appear to be genuinely young objects. Not only do they have the smallest dynamical ages observed, on the order of 100 yr (see Fig. 8), but they also tend to be the most luminous objects. Since Figure 8 and equation (6) imply that high-density, high-excitation class objects should have greater dynamical ages than the low-excitation class objects, the diagram cannot be ascribed to selection effects. If these objects existed, we would see them. We must therefore conclude that the upper boundary observed on the excitation class/density plane is determined by the evolutionary track of the most massive PNn in this diagram. This supposition is confirmed by the fact that the low- excitation/high-density objects are also the most luminous, as would be expected to be the case with massive PNn. Conversely, the fainter, low-density, low-excitation objects have long dynamical time scales and therefore probably originate from low-mass PNn, which only evolve slowly in the H-R diagram. We therefore postulate that, at a given mass for the PNn, the evolutionary tracks of constant PNn mass in the excitation class/density plane (Fig. 6) are from lower right to upper left, approximately parallel to the upper envelope of points. If this is the case, then

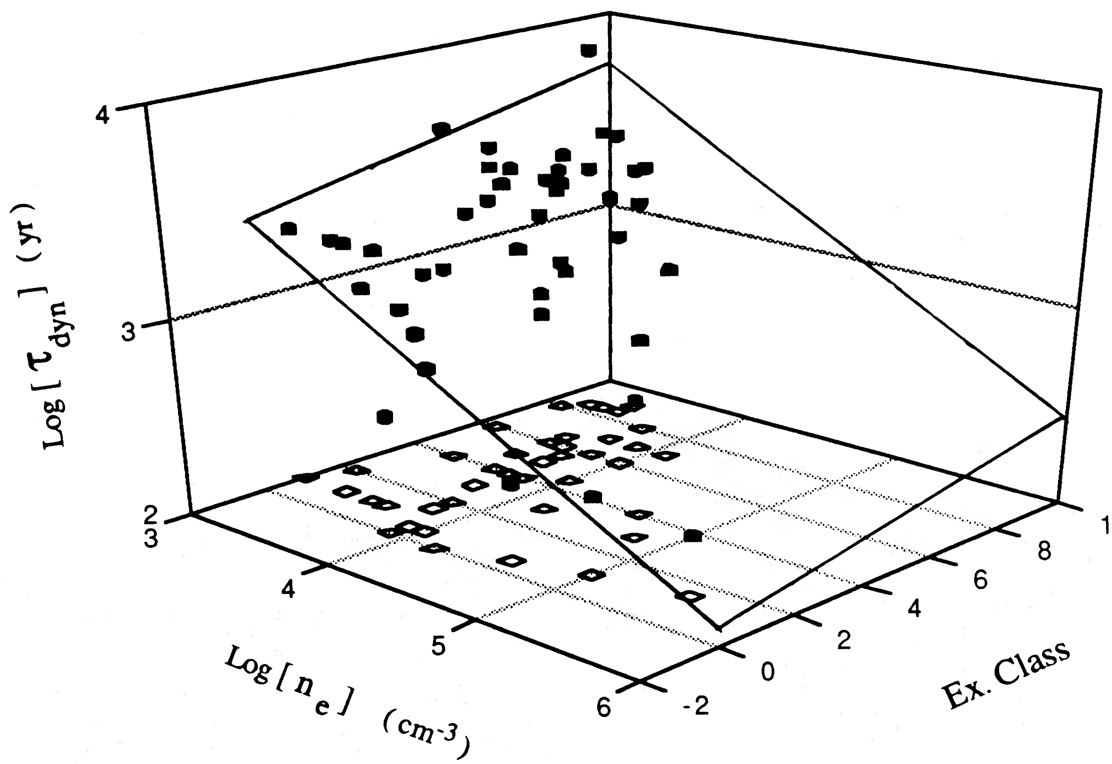

FIG. 8.—The evolutionary plane in terms of the density and excitation class. The observed points are shown in black with their projections onto the (x, y)-plane as open squares. The observed points define a tilted plane shown in outline.

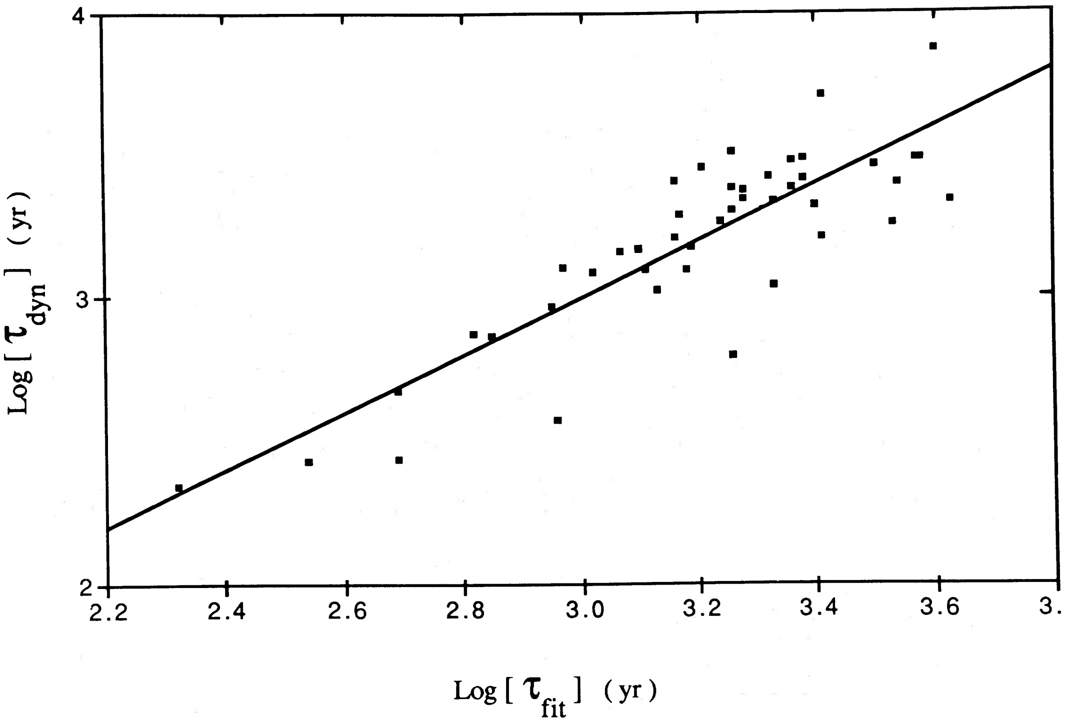

FIG. 9.—The dynamical age given by equation (6) compared with the "observed" dynamical age. The scatter is sufficiently small that this could be used as a new method for determining the distances of Galactic PN.

the type I planetaries (Greig 1971; Peimbert 1978) might be expected to occur preferentially close to this upper envelope, since these are thought to come from massive precursors. This certainly appears to be the case. Objects known to be of type I on the basis of their spectra (in particular, the strength of nitrogen lines or the abundance derived for this element) are marked as larger symbols in Figure 6. These include LMC SMP 83 (see Dopita, Ford, and Webster 1985), SMC SMP 21, 22, 28, and LMC SMP 21 and 29, all classified as type I by Barlow (1986).

The implication of Figure 8, that the population of PN in the Magellanic Clouds is a two-parameter family with little intrinsic scatter, could be of great value in the solution of the thorny question of the Galactic distance scale for PN. Most past studies have used the Shlovsky method, which relies on the assumption of constant nebular mass and a measurement of angular radius and Hβ flux to obtain distance (see, e.g., O'Dell 1962; Seaton 1968; Cahn and Kaler 1971). In its original formulation this method is now largely discredited since it has been recognized that, for optically thick objects, the ionized mass is a widely variable quantity (see, for example, Fig. 7), and the more recent statistical distance scales are based on empirical relationships between ionized mass and nebular radius (Daub 1982; Maciel and Pottasch 1980; Maciel 1981, 1984; Amnuel *et al.* 1984). However, even assuming that this relation is properly calibrated, the statistical uncertainty is fairly large, of order 0.25 in the logarithm for nebular sizes smaller than 0.1 pc, and increasing rapidly for larger nebulae (Wood *et al.* 1987). However, Figures 8 and 9 imply that we could derive a distance simply from a knowledge of excitation class, electron density in the [O II] zone, and a determination of the expansion velocity. Since none of these quantities is affected by reddening, the technique should be more reliable. It should also be somewhat more accurate. The mean scatter of points in Figure 9 is only 0.17 in the logarithm. Since the expansion velocity can be measured with very little error, except in the case of the bipolar nebulae, the mean error in the derived distance will also be of this order, about 40%. This promising new distance indicator will be investigated in a future paper.

VI. CONCLUSIONS

Expansion velocities in both the [O III] and [O II] lines, and electron densities in the [O II] lines, have been determined for many nebulae in the Large Magellanic Cloud. Correlations have been found between quantities determined largely by the central star (luminosity, excitation) and the nebular parameters (expansion velocity, nebular momentum, and dynamical age). These give clear observational evidence that the planetary nebular shell parameters are determined *only* by the parameters if the central star, a fact which will much simplify the construction of theoretical models. This fact also suggests a new method for determining the distances of Galactic PN.

REFERENCES

Aller, L. H. 1956, *Gaseous Nebulae* (New York: Wiley)
Amnuel, P. R., Guseinov, O. H., Novruzova, H. I. and Rustamov, Yu. S. 1984, *Ap. Space Sci.*, **107**, 19.
Barlow, M. J. 1987 *M.N.R.A.S.*, **227**, 161.
Bohuski, T. J., and Smith, M. J. 1974, *Ap. J.*, **193**, 197.
Cahn, J. H., and Kaler, J. B. 1971, *Ap. J. Suppl.*, **22**, 319.
Daub, C. T. 1982, *Ap. J.*, **260**, 612.
Dopita, M. A., Ford, H. C., Lawrence, C. J., and Webster, B. L. 1985, *Ap. J.*, **296**, 390 (DFLW).
Dopita, M. A., Ford, H. C., and Webster, B. L. 1985, *Ap. J.*, **297**, 593.
Dopita, M. A., Meatheringham, S. J., Wood, P. R., Webster, B. L., Morgan, D. H., and Ford, H. C. 1987*a*, *Ap. J.* (*Letters*), **315**, L107.
Dopita, M. A., Meatheringham, S. J., Morgan, D. H., Webster, B. L., and Ford, H. C. 1987*b*, in preparation.

Dyson, J. E. 1981, in *Investigating the Universe*, ed. F. D. Kahn (Dordrecht: Reidel), p. 125.
Feast, M. W. 1968, *M.N.R.A.S.*, **140**, 345.
Grieg, W. E. 1971, *Astr. Ap.*, **10**, 161.
Henize, K. G., and Westerlund, B. E. 1963, *Ap. J.*, **137**, 747.
Jacoby, G. H. 1980, *Ap. J. Suppl.*, **42**, 1.
Maciel, W. J. 1981, *Astr. Ap. Suppl.*, **44**, 123.
———. 1984, *Astr. Ap. Suppl.*, **55**, 253.
Maciel, W. J., and Pottasch, S. R. 1980, *Astr. Ap.*, **88**, 1.
Meatheringham, S. J., Dopita, M. A., Ford, H. C., and Webster, B. L. 1988, *Ap. J.*, **327**, 651.
Meatheringham, S. J., Dopita, M. A., and Morgan, D. H. 1988, *Ap. J.*, in press.
Morgan, D. H. 1984, *M.N.R.A.S.*, **208**, 633.
Morgan, D. H., and Good, A. R. 1985, *M.N.R.A.S.*, **213**, 491 (MG).
O'Dell, C. R. 1962, *Ap. J.*, **135**, 371.
Peimbert, M. 1978, in *IAU Symposium 76, Planetary Nebulae*, ed. Y. Terzian (Dordrecht: Reidel), p. 215.
Pelat, D., Alloin, D., and Fosbury, R. A. E. 1981, *M.N.R.A.S.*, **195**, 787.
Phillips, J. P. 1984, *Astr. Ap.*, **137**, 92.
Pottasch, S. R. 1980, *Astr. Ap.*, **89**, 336.
Pradhan, A. K. 1976, *M.N.R.A.S.*, **177**, 31.
Robinson, G. J., Reay, N. K., and Atherton, P. D. 1982, *M.N.R.A.S.*, **199**, 649.
Sabbadin, F. 1986*a*, *Astr. Ap.*, **160**, 31.
———. 1986*b*, *Astr. Ap.*, **164**, 579.
Sabbadin, F., Bianchini, A., and Hamzaoglu, E. 1984, *Astr. Ap.*, **136**, 200.
Sabbadin, F., Gratton, R. G., Bianchini, A., and Ortolani, S. 1984, *Astr. Ap.*, **136**, 181.
Sabbadin, F., and Hamzaoglu, E. 1982, *Astr. Ap.*, **110**, 105.
Sanduleak, N., McConnell, D. J., and Philip, A. G. D. 1978, *Pub. A.S.P.*, **90**, 621 (SMP).
Seaton, M. J. 1966, *M.N.R.A.S.*, **132**, 113.
———. 1968, *Ap. Letters*, **2**, 55.
Smith, H. C. 1969, M. A. thesis, University of Virginia.
Wilson, O. C. 1950, *Ap. J.*, **111**, 279.
Wood, P. R., Bessell, M. S., and Dopita, M. A. 1985, *Proc. Astr. Soc. Australia*, **6**, 54.
Wood, P. R., Dopita, M. A., and Bessell, M. S. 1986, *Ap. J.*, **311**, 632.
Wood, P. R., and Faulkner, D. J. 1986, *Ap. J.*, **307**, 659.
Wood, P. R., Meatheringham, S. J., Dopita, M. A., and Morgan, D. H. 1987, *Ap. J.*, **320**, 178.
Zeippen, C. J. 1982, *M.N.R.A.S.*, **198**, 111.

MICHAEL A. DOPITA and STEPHEN J. MEATHERINGHAM: Mt. Stromlo and Siding Spring Observatories, Australian National University, Private Bag, Woden P.O., ACT 2606, Australia

HOLLAND C. FORD: Space Telescope Science Institute, Homewood Campus, Baltimore, MD 21218

B. LOUISE WEBSTER: School of Physics, University of New South Wales, P.O. Box 1, Kensington, NSW 2033, Australia